A Reactive Collision Avoidance Algorithm for Nonholonomic Vehicles

Martin S. Wiig[1,2], Kristin Y. Pettersen[1,2] and Andrey V. Savkin[3]

Abstract— This paper presents a reactive collision avoidance algorithm for vehicles with unicycle-type nonholonomic constraints. Static and dynamic obstacles are avoided by keeping a constant avoidance angle to the obstacle. The algorithm compensates for the obstacle velocity, which can be time-varying. Conditions are derived under which successful collision avoidance is mathematically proved, and the theoretical results are supported by simulations. The proposed algorithm makes only limited sensing requirements of the vehicle. It is intuitive, has a low computational complexity and is suitable also for vehicles with a limited speed envelope or heavy linear acceleration constraints. This is demonstrated by applying the algorithm to a vehicle with a constant forward speed.

I. INTRODUCTION

Autonomous vehicles are increasingly used in both scientific and commercial applications. During autonomous or semi-autonomous operations, the capability to avoid static and dynamic obstacles without human intervention is crucial for mission success and vehicle safety. The development and analysis of collision avoidance (CA) algorithms is thus an important and vital field in robotics research.

Reviews of different CA approaches are given in [1] and [2]. The different approaches can generally be divided into two groups [3]; motion planning algorithms and reactive algorithms. The general motion planning problem with bounded velocities and multiple obstacles has been shown to be NP-hard [4]. It is possible to bound the problem to make it more tractable [5], but it might still be unfeasible for vehicles with limited processing power to apply real time motion planning. This is particularly the case in uncertain and dynamic environments, which can require a high replanning frequency. Such vehicles should therefore employ reactive algorithms.

A much used reactive approach is to use artificial potential fields to create control inputs for obstacle avoidance [6]. The method has some stability issues [7], which the vector field histogram [8] seeks to counter by choosing a safe direction from a polar histogram of merged sensor measurements. Another potential field approach is the navigation vector field [9], where local minima are avoided by directly creating a gradient field with this in mind.

[1]Centre for Autonomous Marine Operations and Systems (NTNU AMOS), Department of Engineering Cybernetics, Norwegian University of Science and Technology, 7491 Trondheim, Norway. `Martin.Wiig@ntnu.no`

[2]Norwegian Defence Research Establishment (FFI), P.O. Box 25, N-2027 Kjeller, Norway.

[3]School of Electrical Engineering and Telecommunications, The University of New South Wales, Sydney 2052, Australia

The potential field methods consider only static obstacles, and the performance of vehicles with nonholonomic constraints is rarely analyzed. The dynamic window algorithm [10], [11] incorporates such constraints by searching through a set of valid vehicle trajectories to find a safe control input. Again, only static obstacles are considered.

The velocity obstacle [12] and collision cone [13] approaches deal with moving obstacles. However, they do not consider vehicles with nonholonomic kinematic constraints. The generalized velocity obstacle [14] compensates for nonholonomic kinematics by defining the velocity obstacle in terms of safe control inputs to the vehicle. A sampling-based approach has to be used to find a safe control, making the algorithm computationally expensive.

The acceleration-velocity obstacle approach [15] introduces acceleration constraints into the velocity obstacle, and can be applied to nonholonomic vehicles moving at nonzero speed. The algorithm proposed by [16] removes the nonholonomic constraints by using input-output linearization. However, both these methods become very restrictive when the linear acceleration bound is much more strict than the bound on angular acceleration, which can be the case for vehicles such as fixed-wing aircraft.

A local, range-only-based CA algorithm for nonholonomic vehicles is proposed in [17], which considers moving obstacles of arbitrary and time-varying shapes. The sensing requirements on a vehicle using the algorithm in [17] is very limited, however the algorithm places heavy restrictions on the obstacle velocities.

The algorithm presented in [18] resembles the vector field histogram [8], and uses sensor measurements directly to obtain obstacle-free directions ahead of the vehicle. It is proved that the algorithm makes a nonholonomic vehicle safely traverse a complex environment with multiple moving obstacles. The algorithm does not, however, make use of the obstacle velocity, something which can give overly conservative restrictions to obstacle movement in cases where obstacle velocity measurements are available. Such measurements are indeed not always available, but can be obtained for example by using a lidar or sonar able to measure Doppler shift. In this paper, the obstacle velocity is assumed to be available, and the algorithm we propose make use of it.

Another reactive algorithm for nonholonomic vehicles is presented in [19], where a constant avoidance angle is maintained between the vehicle heading and the tangent from the vehicle to the obstacle. The algorithm makes use of the obstacle velocity, has a low computational complexity and limited vehicle sensing requirements. It is mathematically proved that the vehicle avoids obstacles moving with constant

velocity, however the analysis does not consider time-varying obstacle velocity.

The algorithm proposed by [19] varies the vehicle speed as it circles around the obstacle, and can in some cases make the vehicle almost stop. This can be unfortunate for vehicles with a limited speed envelope, such as fixed-wing aircraft. Other vehicles, such as many marine vehicles, have a very large inertia which restricts the linear acceleration. For such vehicles, it is preferable to apply CA algorithms that maintain a constant forward speed. Reactive CA algorithms that maintain a constant forward speed for cooperating nonholonomic vehicles are given in [20]–[22]. However, in a real world scenario the obstacles may not always be other cooperating agents. There is thus a need for an algorithm that lifts this assumption.

The main contribution of this paper is a reactive CA algorithm for nonholonomic vehicles. The algorithm builds on the work in [19], making the vehicle maintain a constant avoidance angle to the obstacle. However, the algorithm we propose only steers the heading of the vehicle, and is decoupled from vehicle speed, allowing the vehicle to maintain a constant forward speed. It is thus more suitable for vehicles with a limited speed envelope or heavy linear acceleration constraints. To show the applicability to such vehicles, we apply the algorithm to a vehicle that is restricted to keep a constant forward speed. The algorithm can also be used on vehicles without such restrictions, which will then give a large amount of flexibility in designing the desired speed trajectory. Since the proposed algorithm only uses measurements that can be obtained more or less directly from the sensor, and uses few calculations to obtain the desired heading, it has a low computational complexity.

Unlike the works presented in [20]–[22], which assume cooperating obstacles, and the analysis in [19], which only considers obstacles moving at constant speed, we make very few assumptions on the overall obstacle behavior. Indeed, the obstacle might even be actively pursuing the vehicle. The only assumption made on the obstacle velocity is that its maximum speed is less than the vehicle speed. A mathematical analysis is applied to derive a lower bound on the maximum vehicle turning rate required to guarantee avoidance of a circular obstacle with time-varying velocity. The implementation of the algorithm does not, however, require knowledge of the obstacle shape. Only the angles from the vehicle to the outermost edges of the obstacle are required in addition to the obstacle velocity.

Another contribution of the paper is the introduction of an extended vision cone, which defines the sets of safe and unsafe directions at the current vehicle speed and is used to define the criterion for transition between guidance mode and CA mode.

The remainder of this paper is organized as follows. Section II describes the vehicle and obstacle models, the sensing model and the control objective of the system. Section III states the heading controller and the target reaching guidance law employed when the vehicle is not in CA mode. Section IV describes the CA algorithm, and the CA property

of the system is mathematically proved in Section V. The analysis is supported by simulations in Section VI. Finally, concluding remarks are given in Section VII.

II. SYSTEM DESCRIPTION

A. Vehicle model

The vehicle is modeled as a unicycle-type vehicle,

$$\dot{x}(t) = u\cos(\psi(t)), \qquad x(0) = x_0, \qquad (1a)$$
$$\dot{y}(t) = u\sin(\psi(t)), \qquad y(0) = y_0, \qquad (1b)$$
$$\dot{\psi}(t) = r(t), \qquad \psi(0) = \psi_0, \qquad (1c)$$

where $x(t)$ and $y(t)$ are the vehicle's Cartesian coordinates, u is the forward speed, and $\psi(t)$ and $r(t)$ are the heading and heading rate, respectively. The vehicle position is denoted $\boldsymbol{p}(t) \triangleq [x(t), y(t)]^T$.

Assumption 1: The vehicle forward speed $u > 0$ is constant.

Assumption 2: The heading rate $r(t)$ is directly controlled, and bounded by

$$r(t) \in [-r_{\max}, r_{\max}], \qquad (2)$$

where $r_{\max} > 0$ is a constant vehicle parameter.

B. Obstacle model

The obstacle is modeled as a nonholonomic vehicle,

$$\dot{x}_o(t) = u_o(t)\cos(\psi_o(t)), \qquad x_o(0) = x_{o,0}, \qquad (3a)$$
$$\dot{y}_o(t) = u_o(t)\sin(\psi_o(t)), \qquad y_o(0) = y_{o,0}, \qquad (3b)$$
$$\dot{\psi}_o(t) = r_o(t), \qquad \psi_o(0) = \psi_{o,0}, \qquad (3c)$$
$$\dot{u}_o(t) = a_o(t), \qquad u_o(0) = u_{o,0}, \qquad (3d)$$

where $x_o(t)$ and $y_o(t)$ are the Cartesian coordinates of the obstacle, $u_o(t)$ and $a_o(t)$ are the forward speed and acceleration, and $\psi_o(t)$ and $r_o(t)$ are the obstacle heading and heading rate. The obstacle velocity vector is defined as $\boldsymbol{v}_o(t) \triangleq [\dot{x}_o(t), \dot{y}_o(t)]^T$.

Assumption 3: The obstacle is modeled as a moving circular domain $D_o(t)$ of radius R_o with center at $[x_o(t), y_o(t)]^T$.

Remark 1: The CA algorithm presented in this paper can also be applied to non-circular obstacles, as shown in the last simulation scenario in Section VI.

Assumption 4: The obstacle forward speed $u_o(t)$ is bounded by

$$0 \leq u_o(t) \leq u_{o,\max} < u. \qquad (4)$$

Assumption 5: The obstacle forward acceleration $a_o(t)$ is bounded by

$$a_o(t) \in [-a_{o,\max}, a_{o,\max}], \qquad (5)$$

where $a_{o,\max} > 0$ is a constant parameter.

Assumption 6: The obstacle heading rate $r_o(t)$ is bounded by

$$r_o(t) \in [-r_{o,\max}, r_{o,\max}], \qquad (6)$$

where $r_{o,\max} > 0$ is a constant parameter.
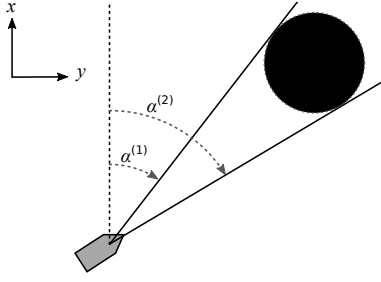
Fig. 1. The vision cone from the vehicle to the obstacle

C. Sensing model

This section describes the obstacle measurements needed to implement the CA algorithm. The minimum distance $d_o(t)$ between the vehicle and the obstacle at time t is defined as

$$d_o(t) := \min_{\boldsymbol{p}_D \in D_o(t)} ||\boldsymbol{p}_D - \boldsymbol{p}(t)||, \qquad (7)$$

where $|| \cdot ||$ denotes the Euclidean norm. The vehicle is able to measure both $d_o(t)$ and $\dot{d}_o(t)$ when the obstacle is within a sensing range $d_{\text{sense}} > 0$. Furthermore, the vehicle is able to measure the angles $\alpha^{(1)}(t)$ and $\alpha^{(2)}(t)$ between the x-axis and the sides of the vision cone from the vehicle to the obstacle, as shown in Figure 1. Finally, the vehicle is able to measure the obstacle velocity $\boldsymbol{v}_o(t) = [\dot{x}_o(t), \dot{y}_o(t)]^T$.

D. Control objective

The objective of the control system and the CA algorithm is to make the vehicle reach a target position $\boldsymbol{p}_t = [x_t, y_t]^T$ at some unspecified time $t_f \in [0, \infty)$:

$$\boldsymbol{p}(t_f) = \boldsymbol{p}_t. \qquad (8)$$

This goal should be achieved while keeping at least a minimum safety distance d_{safe} to the obstacle:

$$d_o(t) \geq d_{\text{safe}} > 0 \quad \forall t \in [0, t_f]. \qquad (9)$$

III. CONTROL SYSTEM

The control system has two modes; guidance mode and CA mode. In guidance mode, the guidance law given in Section III-B makes the vehicle move straight towards the target. If the obstacle comes within range and the desired heading from the guidance law is unsafe, the control system enters CA mode. This switch is described in Section IV-C. The desired heading is then given by the CA law presented in Section IV.

A. Heading controller

To make the vehicle reach the target heading as fast as possible, it is made to turn towards the desired heading ψ_d at the maximum turning rate:

$$r(\psi_d) \triangleq \begin{cases} 0 & \tilde{\psi} = 0 \\ r_{\max} & \tilde{\psi} \in (-\pi, 0) \\ -r_{\max} & \tilde{\psi} \in (0, \pi]. \end{cases} \qquad (10)$$

The heading error variable $\tilde{\psi} \triangleq \psi - \psi_d$ is chosen to belong to the interval $\tilde{\psi} \in (-\pi, \pi]$, to ensure that the vehicle always makes the shortest turn towards ψ_d.

B. Guidance law

When the control system is in guidance mode, the heading is guided by a pure pursuit guidance law [23]:

$$\psi_{\text{dg}}(t) \triangleq \text{atan2}\left(y_t - y(t), x_t - x(t)\right), \qquad (11)$$

where $\psi_{\text{dg}} \in [0, 2\pi)$ is the desired heading. The pure pursuit law directs the vehicle straight towards the target position $\boldsymbol{p}_t$, and has the nice property that the heading reference will not change once $\psi(t) = \psi_{\text{dg}}(t)$, which simplifies the analysis of the system in Section V.

IV. COLLISION AVOIDANCE ALGORITHM

In this section we propose a CA algorithm that makes the vehicle maintain a constant avoidance angle $\alpha_o \in (0, \frac{\pi}{2})$ to one of the tangent lines between the vehicle and the obstacle. The vehicle keeps a constant forward speed while maintaining the avoidance angle, and the algorithm compensates for obstacle velocity.

For clarity of exposition, a static obstacle is considered first. The algorithm is then extended to include a moving obstacle. The rule for switching between nominal guidance and CA is defined in Section IV-C, while Section IV-D gives a criterion for moving in a clockwise or counter-clockwise direction around the obstacle.

A. Static obstacle

To obtain headings keeping the avoidance angle α_o to the tangents from the vehicle to the obstacle, the vision cone is extended by α_o as shown in Figure 2. The direction of the sides of the extended vision cone are denoted $\beta^{(1)}$ and $\beta^{(2)}$.
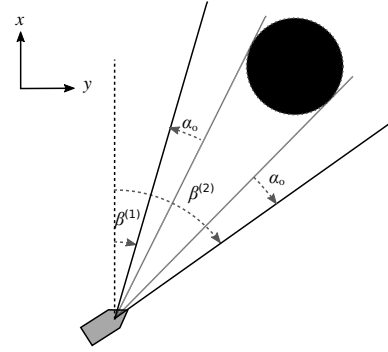
Fig. 2. The extended vision cone from the vehicle to the obstacle

Two velocity vectors $\boldsymbol{v}_{\beta^{(1)}}$ and $\boldsymbol{v}_{\beta^{(2)}}$ are defined along the sides of the extended vision cone as

$$\boldsymbol{v}_{\beta^{(j)}}(t) := u_{\beta^{(j)}}(t) \left[\cos(\beta^{(j)}(t)), \sin(\beta^{(j)}(t))\right], \qquad (12)$$

where $j = \{1, 2\}$. In order to make the vehicle keep the constant forward speed, $u_{\beta^{(j)}}(t) \triangleq u$. The candidates for the desired heading in order to avoid collision are thus

$$\psi_{\text{dca}}^{(j)}(t) = \beta^{(j)}(t), \ j = \{1, 2\}. \qquad (13)$$

In Section IV-D we present a criterion for choosing between these two candidates.

Note that, when the obstacle is considered static, the proposed CA law and the one presented in [19] both reduce to the same form.

B. Moving obstacle

To avoid a moving obstacle, the proposed CA algorithm will make the vehicle keep the velocity $\boldsymbol{v}_{\beta(j)}(t)$, given in (12), in a non-rotating coordinate frame moving with the obstacle velocity $\boldsymbol{v}_{\mathrm{o}}(t)$. In order to achieve this, a compensated vision cone $\mathcal{V}_{\mathrm{o}}(t)$ is defined by compensating the extended vision cone for the obstacle velocity $\boldsymbol{v}_{\mathrm{o}}(t)$, as illustrated in Figure 3. The velocity vectors defining the sides of $\mathcal{V}_{\mathrm{o}}$ are
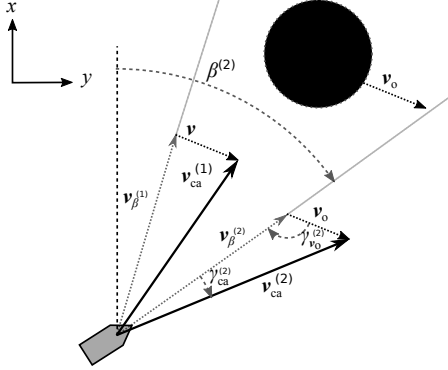
Fig. 3. The desired velocity vector candidates $\boldsymbol{v}_{\mathrm{ca}}^{(1)}$ and $\boldsymbol{v}_{\mathrm{ca}}^{(2)}$, which defines the compensated vision cone $\mathcal{V}_{\mathrm{o}}$.

then given by

$$\boldsymbol{v}_{\mathrm{ca}}^{(j)}(t) \triangleq \boldsymbol{v}_{\beta(j)}(t) + \boldsymbol{v}_{\mathrm{o}}(t). \qquad (14)$$

These are the candidates for the desired velocity of the vehicle in CA. Since the vehicle keeps a constant forward speed u, the length of the velocity vector is set to $\|\boldsymbol{v}_{\mathrm{ca}}^{(j)}(t)\| \triangleq u$. From Figure 3, the angle $\gamma_{\boldsymbol{v}_{\mathrm{o}}}^{(j)}(t)$ between $\boldsymbol{v}_{\beta(j)}(t)$ and $\boldsymbol{v}_{\mathrm{o}}(t)$ can be seen to be

$$\gamma_{\boldsymbol{v}_{\mathrm{o}}}^{(j)}(t) = \pi - (\psi_{\mathrm{o}}(t) - \beta^{(j)}(t)), \; j = \{1,2\}, \qquad (15)$$

where $\psi_{\mathrm{o}}(t)$ is the direction of $\boldsymbol{v}_{\mathrm{o}}(t)$ as defined in (3). The sine rule can then be used to find the angle $\gamma_{\mathrm{ca}}^{(j)}(t)$ between $\boldsymbol{v}_{\beta(j)}(t)$ and $\boldsymbol{v}_{\mathrm{ca}}^{(j)}(t)$:

$$\gamma_{\mathrm{ca}}^{(j)}(t) = \sin^{-1}\left(\frac{u_{\mathrm{o}}(t)\sin(\gamma_{\boldsymbol{v}_{\mathrm{o}}}^{(j)}(t))}{u}\right), \; j = \{1,2\}. \qquad (16)$$

The CA law for avoiding a moving obstacle is then given by (17):

$$\psi_{\mathrm{dca}}^{(j)}(t) = \beta^{(j)}(t) + \gamma_{\mathrm{ca}}^{(j)}(t), \; j = \{1,2\}. \qquad (17)$$

Compared to the CA law given in (13) for avoiding a static obstacle, the desired heading compensates for $\boldsymbol{v}_{\mathrm{o}}(t)$ by the addition of $\gamma_{\mathrm{ca}}^{(j)}(t)$.

Remark 2: The term $\gamma_{\mathrm{ca}}^{(j)}(t)$ is bounded by $\pm\sin^{-1}(u_{\mathrm{o,max}}/u)$. This bound can be used in (17) if the obstacle velocity is not available. It is then also possible to use a CA algorithm designed to not include obstacle velocity, like the one presented in [18].

C. Switching rule

We define that the vehicle enters CA mode at a time t_1 if the obstacle is closer than or equal to a chosen range, d_{switch}, and the heading $\psi_{\mathrm{dg}}(t_1)$ from the nominal heading guidance law in (11) is within the compensated vision cone $\mathcal{V}_{\mathrm{o}}(t_1)$:

$$\psi_{\mathrm{dg}}(t_1) \in \mathcal{V}_{\mathrm{o}}(t_1), \qquad (18)$$
$$d_{\mathrm{o}}(t_1) \leq d_{\mathrm{switch}} \in (d_{\mathrm{safe}}, d_{\mathrm{sense}}]. \qquad (19)$$

Nominal guidance towards the target will resume at a time t_2 when $\psi_{\mathrm{dg}}(t_2)$ moves outside $\mathcal{V}_{\mathrm{o}}(t_2)$, i.e. when $\psi_{\mathrm{dg}}(t_2)$ can be considered safe:

$$\psi_{\mathrm{dg}}(t_2) \notin \mathcal{V}_{\mathrm{o}}(t_2). \qquad (20)$$

D. Turning direction

The proposed CA algorithm (17) provides two alternative candidates for the desired heading in order to avoid collision. We will use this flexibility to make the vehicle seek to move behind the obstacle. In particular, we choose the following direction parameter j when the vehicle enters CA mode:

$$j = \begin{cases} \arg\max_{j=1,2} & |\psi_{\mathrm{o}}(t) - \psi_{\mathrm{dca}}^{(j)}(t)|, \quad d_{\mathrm{o}}(t) = d_{\mathrm{switch}}, \\ \arg\min_{j=1,2} & |\psi(t) - \psi_{\mathrm{dca}}^{(j)}(t)|, \quad d_{\mathrm{o}}(t) < d_{\mathrm{switch}}. \end{cases} \qquad (21)$$

When $d_{\mathrm{o}}(t) = d_{\mathrm{switch}}$ this maximizes the difference between the obstacle heading and the CA direction. However, if the obstacle is closer than d_{switch} when the vehicle enters CA mode, the vehicle will make the shortest turn towards a safe direction. This can for instance happen if a nearby obstacle turns so that the current vehicle heading becomes unsafe.

Remark 3: The algorithm avoids collisions regardless of the method used to choose j when $d_{\mathrm{o}}(t) = d_{\mathrm{switch}}$.

V. MATHEMATICAL ANALYSIS

This section presents a mathematical analysis of the closed-loop control system (1), (10), including the switching between guidance mode where ψ_{d} in (10) is given by (11), and CA mode where ψ_{d} is given by (17), according to the switching rule in Section IV-C. In particular, for a static obstacle we will show, as stated in the following lemma, that a vehicle maintaining $\boldsymbol{v}_{\beta(j)}(t)$ (12) will converge to a circle around the obstacle. Lemma 2 gives a bound on the angular velocity of $\psi_{\mathrm{dca}}^{(j)}$ given by (17) when avoiding a moving obstacle. These lemmas are then used in the proof of Theorem 1, which states that the control objectives (8) and (9) are met for a vehicle (1) controlled by the controller (10), guidance law (11) and CA law (17), in the presence of an obstacle with time-varying velocity.

Lemma 1: If the obstacle is static and $\alpha_{\mathrm{o}} \in (0, \frac{\pi}{2})$, then a vehicle described by (1) maintaining the velocity $\boldsymbol{v}_{\beta(j)}(t)$ (12) with forward speed $u_{\beta(j)}(t) > 0$ converges to a circle $\mathcal{C}$ with center at the obstacle center and radius $\frac{R_{\mathrm{o}}}{\cos(\alpha_{\mathrm{o}})}$. Furthermore, if the vehicle starts outside $\mathcal{C}$, then

$$d_{\mathrm{o}}(t) \geq d_{\min} \triangleq \frac{R_{\mathrm{o}}}{\cos(\alpha_{\mathrm{o}})} - R_{\mathrm{o}}, \quad \forall t \geq 0 \qquad (22)$$

Proof: A vehicle moving with velocity $\boldsymbol{v}_{\beta(j)}(t)$ maintains the avoidance angle α_{o} to one of the tangent lines from
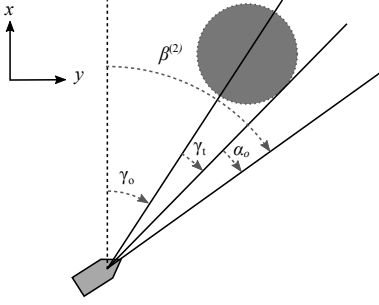
Fig. 4.   Decomposition of $\beta^{(2)}$.

the vehicle to the obstacle, as shown in Figure 2. The distance between the vehicle and the obstacle thus evolves as

$$\dot{d}_o(t) = -u_{\beta^{(j)}}(t)\cos(\gamma_t(t) + \alpha_o), \qquad (23)$$

where $u_{\beta^{(j)}}(t)$ is the length of $\boldsymbol{v}_{\beta^{(j)}}(t)$ given by (12), and $\gamma_t(t) > 0$ is the angle from the line connecting the vehicle and the center of the obstacle to the tangent line as seen in Figure 4. It follows that $\dot{d}_o(t) < 0$ when $\gamma_t(t) + \alpha_o < \frac{\pi}{2}$, which occurs when $d_o(t) > d_{\min}$. Furthermore, $\dot{d}_o(t) > 0$ when $d_o(t) < d_{\min}$, and $\dot{d}_o(t) = 0$ when $d_o(t) = d_{\min}$. Hence, the vehicle will converge to $\mathcal{C}$, and if the vehicle starts outside $\mathcal{C}$ then $d_o(t) \geq d_{\min} \ \forall t \geq 0$.   ∎

It follows from Lemma 1 that if the avoidance angle α_o is chosen to satisfy

$$\alpha_o \geq \cos^{-1}\left(\frac{R_o}{R_o + d_{\text{safe}}}\right) \qquad (24)$$

then, under the conditions that the obstacle static, the vehicle starts outside $\mathcal{C}$ and keeps the velocity $\boldsymbol{v}_{\beta^{(j)}}(t)$ from (12),

$$d_o(t) \geq d_{\text{safe}} \quad \forall t \geq 0. \qquad (25)$$

To ensure that the vehicle is able to follow $\psi_{\text{dca}}^{(j)}(t)$ (17), it is required that $r_{\max} \geq |\dot{\psi}_{\text{dca}}^{(j)}(t)|$ during the CA maneuver. The following lemma gives a bound on $|\dot{\psi}_{\text{dca}}^{(j)}(t)|$ that holds both for static and dynamic obstacles:

Lemma 2: Consider the vehicle described by (1), and an obstacle modeled by (3). If Assumptions 1 and 3-5 hold, then, for $\psi_{\text{dca}}^{(j)}(t)$ given by (17), $\dot{\psi}_{\text{dca}}^{(j)}(t)$ is bounded by

$$|\dot{\psi}_{\text{dca}}^{(j)}(t)| < \dot{\psi}_{\text{dca,sup}} \triangleq \frac{a_{o,\max}}{\sqrt{u^2 - u_{o,\max}^2}}$$
$$+ \frac{u_{o,\max}}{u}r_{o,\max} + \frac{(u + u_{o,\max})^2}{u\sqrt{(R_o + d_{\text{safe}})^2 - R_o^2}}. \qquad (26)$$

Proof: Without loss of generality, $j = 2$ in the following analysis. Furthermore, the dependency on time will be omitted in the notation. Equation (17) gives

$$\dot{\psi}_{\text{dca}}^{(2)} = \dot{\beta}^{(2)} + \dot{\gamma}_{\text{ca}}^{(2)} \qquad (27)$$

Figure 4 shows that $\beta^{(2)} = \gamma_o + \gamma_t + \alpha_o$, and hence

$$\dot{\beta}^{(2)} = \dot{\gamma}_o + \dot{\gamma}_t. \qquad (28)$$

The angular velocity of γ_o can be found geometrically as

$$\dot{\gamma}_o = \frac{1}{R_o + d_o}\left(u_o \sin(\psi_o - \gamma_o) - u\sin(\psi - \gamma_o)\right). \qquad (29)$$

The tangent angle γ_t is

$$\gamma_t = \sin^{-1}\left(\frac{R_o}{R_o + d_o}\right), \qquad (30)$$

which gives

$$\dot{\gamma}_t = -\dot{d}_o \frac{R_o}{(R_o + d_o)\sqrt{(R_o + d_o)^2 - R_o^2}}. \qquad (31)$$

The time derivative of d_o is found geometrically as

$$\dot{d}_o = u_o \cos(\psi_o - \gamma_o) - u\cos(\psi - \gamma_o). \qquad (32)$$

Combining (29) - (32), applying Assumptions 1 and 4 and maximizing with respect to ψ and ψ_o give the following bound:

$$|\dot{\beta}^{(2)}| = |\dot{\gamma}_o + \dot{\gamma}_t| \leq \frac{u + u_{o,\max}}{\sqrt{(R_o + d_{\text{safe}})^2 - R_o^2}}. \qquad (33)$$

The time derivative of $\gamma_{\text{ca}}^{(2)}$ is found by using (16),

$$\dot{\gamma}_{\text{ca}}^{(2)} = \frac{\dot{u}_o \sin(\gamma_{\boldsymbol{v}_o}^{(2)}) + u_o \cos(\gamma_{\boldsymbol{v}_o}^{(2)})\dot{\gamma}_{\boldsymbol{v}_o}^{(2)}}{\sqrt{u^2 - u_o^2 \sin^2(\gamma_{\boldsymbol{v}_o}^{(2)})}}, \qquad (34)$$

where $\dot{\gamma}_{\boldsymbol{v}_o}^{(2)}$ is found from (15) as

$$\dot{\gamma}_{\boldsymbol{v}_o}^{(2)} = r_o + \dot{\beta}^{(2)}. \qquad (35)$$

Using Assumptions 1 and 4 - 6, $\dot{\gamma}_{\text{ca}}^{(2)}$ is bounded by

$$|\dot{\gamma}_{\text{ca}}^{(2)}| < \frac{a_{o,\max}}{\sqrt{u^2 - u_{o,\max}^2}} + \frac{u_{o,\max}}{u}r_{o,\max} + \frac{u_{o,\max}}{u}|\dot{\beta}^{(2)}|. \qquad (36)$$

Inserting (33) and (36) into (27) gives

$$|\dot{\psi}_{\text{dca}}^{(2)}| < \frac{a_{o,\max}}{\sqrt{u^2 - u_{o,\max}^2}} + \frac{u_{o,\max}}{u}r_{o,\max}$$
$$+ \frac{(u + u_{o,\max})^2}{u\sqrt{(R_o + d_{\text{safe}})^2 - R_o^2}} =: \dot{\psi}_{\text{dca,sup}}, \qquad (37)$$

which concludes the proof.   ∎

Remark 4: The bound (26) on $|\dot{\psi}_{\text{dca}}^{(j)}(t)|$, agrees with intuition. In particular, note that the bound increases as the maximum forward velocity $u_{o,\max}$, acceleration $a_{o,\max}$ and turning rate $r_{o,\max}$ of the obstacle increase.

Before we state the main theorem, we need to make the following assumption to ensure that the target is outside the circle of convergence around the obstacle:

Assumption 7: The distance $d_{o,t}(t)$ from the obstacle to the target position $\boldsymbol{p}_t$ satisfies

$$d_{o,t}(t) > \frac{R_o}{\cos(\alpha_o)} - R_o \qquad \forall t \geq 0, \qquad (38)$$

where $d_{o,t}(t)$ is defined as

$$d_{o,t}(t) \triangleq \min_{\boldsymbol{p}_D \in D_o(t)} ||\boldsymbol{p}_D - \boldsymbol{p}_t||. \qquad (39)$$

Remark 5: Vehicle safety is guaranteed even if this assumption is not met, however it is then not ensured that the target will be reached.

In addition, the vehicle should be able to start safely:

Assumption 8: The initial distance between the vehicle and the obstacle satisfies

$$d_\mathrm{o}(0) > d_\mathrm{switch}. \tag{40}$$

The main theorem is now ready to be stated.

Theorem 1: If Assumptions 1-8 hold, the avoidance angle satisfies

$$\alpha_\mathrm{o} \in \left[\cos^{-1} \left(\frac{R_\mathrm{o}}{R_\mathrm{o}+d_\mathrm{safe}} \right), \frac{\pi}{2} \right), \tag{41}$$

the maximum vehicle turning rate satisfies

$$r_\mathrm{max} \geq \dot{\psi}_\mathrm{dca,sup}, \tag{42}$$

and the switching distance satisfies

$$d_\mathrm{switch} \geq \frac{2u + \pi u_\mathrm{o,max}}{r_\mathrm{max}} + d_\mathrm{safe}, \tag{43}$$

then a vehicle described by (1), controlled by the controller (10), guidance law (11) and CA law (17), will maneuver to $\boldsymbol{p}_\mathrm{t}$ in the presence of an obstacle described by (3) while ensuring that

$$d_\mathrm{o}(t) \geq d_\mathrm{safe} > 0 \quad \forall t \in [0, t_f], \tag{44}$$

where t_f is the time of arrival at $\boldsymbol{p}_\mathrm{t}$.

Proof: The proof follows along the lines of the proof used in [19], which argues that as long as the vehicle is able to follow the desired heading reference from the CA algorithm, it will successfully avoid the obstacle. To achieve this we use the bound on $\dot{\psi}_\mathrm{dca}^{(j)}$ from Lemma 2, along with the switching rule we proposed in Section IV-C.

The switching distance d_switch given in (43) ensures that the vehicle is able to turn $180\,^\circ$ before the obstacle can be within distance d_safe of the vehicle's turning circle. There is then a time t_1 when $d(t_1) >= d_\mathrm{safe}$ and $\psi(t_1) = \psi_\mathrm{dca}(t_1)$. Applying Lemma 2 gives $|\dot{\psi}_\mathrm{dca}^{(j)}(t)| < \dot{\psi}_\mathrm{dca,sup}$. Hence $r_\mathrm{max} \geq |\dot{\psi}_\mathrm{dca}^{(j)}(t)| \ \forall t > 0$, and the vehicle is able to follow (17),

$$\psi(t) = \psi_\mathrm{dca}(t), \forall t \in [t_1, t_2], \tag{45}$$

where t_2 is the time when the vehicle will exit CA.

In a coordinate frame moving with velocity $\boldsymbol{v}_\mathrm{o}$, the vehicle moves with velocity $\boldsymbol{v}_{\beta(j)}(t)$. Hence, the CA algorithm for dynamic obstacles (17) reduces to the one for static obstacles (13), but with varying relative vehicle forward speed $u_{\beta(j)}(t)$. From Figure 3, it can be seen that $u_{\beta(j)}(t)$ achieves minimum when $\gamma_{\boldsymbol{v}_\mathrm{o}}^{(j)} = 0$, for which

$$u_{\beta,\min}^j = u - u_\mathrm{o}(t). \tag{46}$$

Since $u_\mathrm{o}(t) < u$ by Assumption 4, $u_{\beta,\min}^j > 0$. Lemma 1 then implies that the vehicle will converge towards a circle $\mathcal{C}$, which moves with velocity $\boldsymbol{v}_\mathrm{o}$. The circle has radius $\frac{R_\mathrm{o}}{\cos(\alpha_\mathrm{o})}$, and the bound on α_o given in (41) makes

$$d_\mathrm{o}(t) \geq d_\mathrm{safe} \quad \forall t \in [t_1, t_2], \tag{47}$$

which satisfies control objective (9).

Since the vehicle circles around the obstacle, Assumption 7 ensures that there will be a time t_2 when the line of sight to the target $\boldsymbol{p}_\mathrm{t}$ will be outside of $\mathcal{V}_\mathrm{o}$. The vehicle

will then exit CA mode and proceed towards the target. It follows from Lemma 1 that any direction outside of the cone $\mathcal{V}_\mathrm{o}$ ensures that $d_\mathrm{o} > d_\mathrm{safe}$, and hence the direction towards $\boldsymbol{p}_\mathrm{t}$ is safe.

The obstacle may turn so that the line of sight to $\boldsymbol{p}_\mathrm{t}$ comes within $\mathcal{V}_\mathrm{o}$ before $d_\mathrm{o} > d_\mathrm{switch}$, making the vehicle enter CA again. However, since $\boldsymbol{v}_\mathrm{ca}^{(1)}$ and $\boldsymbol{v}_\mathrm{ca}^{(2)}$ are first order differentiable with angular velocity less than $\dot{\psi}_\mathrm{dca,sup}$, and ψ_dca is then chosen to be the closest of $\boldsymbol{v}_\mathrm{ca}^{(1)}$ and $\boldsymbol{v}_\mathrm{ca}^{(2)}$ by (21), the vehicle is immediately able to follow ψ_dca to avoid the obstacle again.

Finally, since $u > u_\mathrm{o,max}$, the vehicle will eventually be able to escape the obstacle and reach the target. This satisfies control objective (8) and concludes the proof. ∎

Remark 6: If the heading rate $r(t)$ is not set instantaneously as assumed in Assumption 2, but rather controlled by a globally exponentially stable controller, the vehicle will still be able to follow the heading reference trajectory from the CA law. The lower bound on the switching distance (43) must then be increased to account for the heading convergence time.

VI. SIMULATIONS

This section presents numerical simulations of three scenarios using the proposed CA algorithm. The first two scenarios contain a circular obstacle of radius $R = 3\,\mathrm{m}$. The third scenario demonstrates the use of the CA algorithm on a convex obstacle. The vehicle speed in all scenarios is set to $u = 1\,\mathrm{m/s}$ and the maximum vehicle turning rate is set to $r_\mathrm{max} = 1\,\mathrm{rad/s}$. The safety distance is set to $d_\mathrm{safe} = 1\,\mathrm{m}$.

The speed of the circular obstacle is set to $u_\mathrm{o} = u_\mathrm{o,max} = 0.7\,\mathrm{m/s}$, while the maximum obstacle acceleration and turning rate are set to $a_\mathrm{o,max} = 0$ and $r_\mathrm{o,max} = 0.15\,\mathrm{rad/s}$. From these parameters (43) gives a minimum switching distance $d_\mathrm{switch,min} = 5.2\,\mathrm{m}$. By Lemma 2, $\dot{\psi}_\mathrm{dca,sup} = 0.98\,\mathrm{s}^{-1}$ for the circular obstacle, and thus $r_\mathrm{max} > \dot{\psi}_\mathrm{dca,sup}$, satisfying (42). Using (24), the minimum offset angle for the circular obstacle is found as $\alpha_\mathrm{o,min} = 41.4\,^\circ$. We choose $\alpha_\mathrm{o} = \alpha_\mathrm{o,min}$ and $d_\mathrm{switch} = d_\mathrm{switch,min}$.

In the first scenario, shown in Figure 5, the vehicle and the obstacle are initially on a head-on collision course where the obstacle moves along a straight trajectory towards the vehicle. At time $t_1 = 6.96\,\mathrm{s}$ the distance to the obstacle satisfies $d(t_1) \leq d_\mathrm{switch}$, and the vehicle enters CA mode. Since the vehicle and the obstacle meets head on, the choice of direction parameter j becomes random. In this particular case $j = 2$ and the vehicle turns to the right.

Figure 6 shows that $|\dot{\psi}_\mathrm{dca}^{(2)}| < \dot{\psi}_\mathrm{dca,sup}$ during the simulation. Hence, since $\dot{\psi}_\mathrm{dca,sup} < r_\mathrm{max}$, the vehicle is able to perfectly follow $\psi_\mathrm{dca}^{(2)}$ after a transition period, which agrees with $r_\mathrm{max} \geq \dot{\psi}_\mathrm{dca,sup}$. The obstacle distance remains greater than d_safe, as seen in the top half of Figure 6. The simulation thus supports the theoretical results given by Theorem 1. At time $13.68\,\mathrm{s}$, the line of sight to the target is outside of the cone $\mathcal{V}_\mathrm{o}(t)$, and the vehicle enters guidance mode. The vehicle then proceeds towards the target in accordance with the pure pursuit guidance law (11).
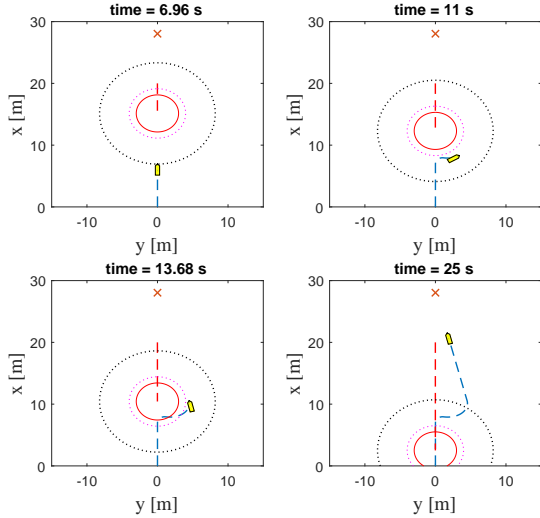
Fig. 5. The first scenario, where the vehicle meets an obstacle head on. The vehicle is the yellow polygon, with $\boldsymbol{p}(t)$ at the nose tip. The obstacle is the solid red circle. The vehicle and obstacle trajectories are the dashed blue and red line, respectively. The dotted magenta circle shows d_{safe}, while the dotted black circle shows d_{switch}. The target is marked by an 'X'.
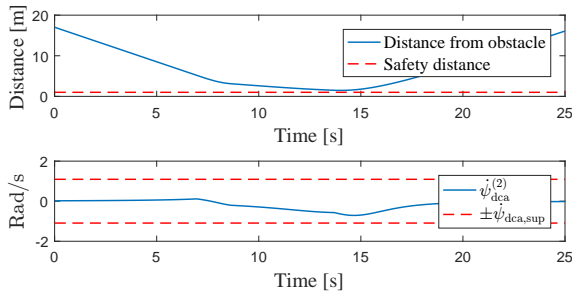
Fig. 6. Distance between the vehicle and the obstacle in the first scenario(top), and the angular velocity of $\psi_{\text{dca}}^{(2)}$ (bottom), which was used during the CA maneuver.

In the second scenario, shown in Figure 7, the obstacle approaches the vehicle along a circular trajectory from the left. The turning rate of the obstacle is set to $r_{\text{o}} = r_{\text{o,max}} = 0.15\,\text{rad/s}$. The vehicle enters CA mode at time $5.49\,\text{s}$, and moves behind the obstacle in accordance with (21).

Figure 8 shows that, like in the first scenario, $|\dot{\psi}_{\text{dca}}^{(1)}| < \dot{\psi}_{\text{dca,sup}}$ and $d(t) \geq d_{\text{safe}}$ during the simulation. Thus, the second simulation also supports the results given in Theorem 1.

The third scenario, shown in Figure 9, contains a concave obstacle moving straight towards the vehicle with speed $u_{\text{o}} = u_{\text{o,max}} = 0.5\,\text{m/s}$. The obstacle consists of two connected arms with circles of radius $3\,\text{m}$ at the extremities. The circle radius was used as input to (24) to obtain $\alpha_{\text{o,min}} = 41.4\,^\circ$, while (43) gives $d_{\text{switch,min}} = 4.57\,\text{m}$, both of which where used in the simulation. At time $22.02\,\text{s}$ the obstacle comes within switching distance. The vehicle travels along the edge of the obstacle until time $50.17\,\text{s}$, when the direction to the
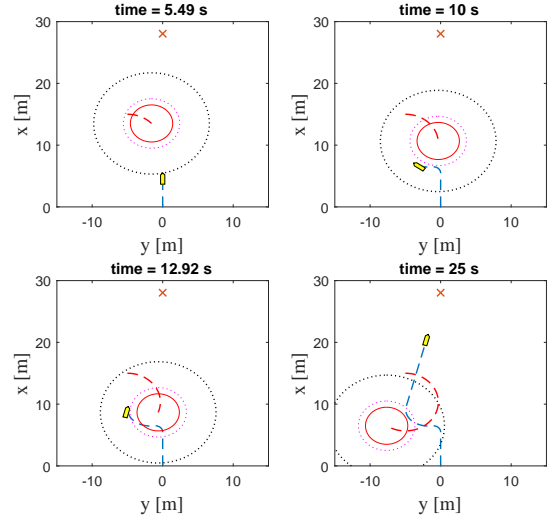
Fig. 7. The second scenario, where the obstacle is moving in a clockwise circle starting to the left of the vehicle.
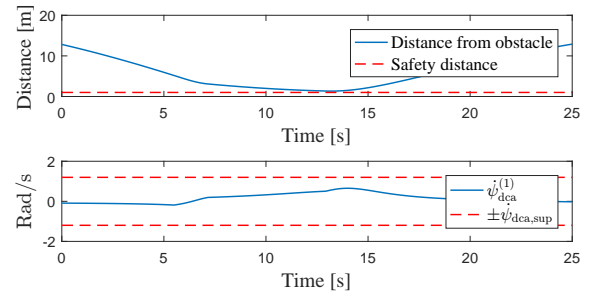
Fig. 8. Distance between the vehicle and the obstacle in the second scenario(top), and the angular velocity of $\psi_{\text{dca}}^{(1)}$ (bottom), which was used during the CA maneuver.

target becomes safe and the vehicle continues towards it. Figure 10 shows that $d(t) \geq d_{\text{safe}}$ during the simulation.

VII. CONCLUSIONS

This paper has presented a reactive collision avoidance algorithm for nonholonomic vehicles. The algorithm makes the vehicle keep a constant avoidance angle to the vision cone from the vehicle to an obstacle. The algorithm compensates for the obstacle velocity, which can be time-varying. The obstacle is not assumed to be cooperating, and might even be in active pursuit of the vehicle. The proposed algorithm is intuitive, has low computational complexity and is suitable for a wide range of vehicles, including vehicles with a limited speed envelope or heavy linear acceleration constraints. This has been demonstrated by applying the algorithm to a vehicle restricted by a constant forward speed.

The main theorem of the paper states the conditions under which it is mathematically proved that a minimum safety distance between the vehicle and the obstacle is not violated. This includes a lower bound on the switching distance and an upper bound on the required vehicle turning rate. The analysis is validated through simulations, which in particular
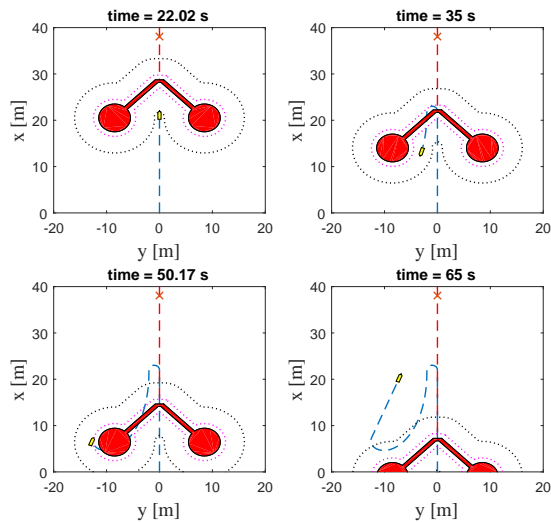
Fig. 9. The third scenario, with a concave obstacle moving straight towards the vehicle
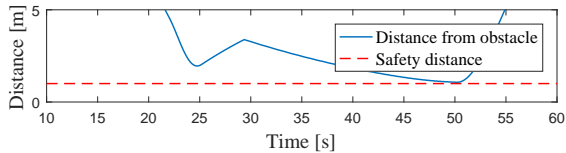
Fig. 10. Distance between the vehicle and the obstacle when avoiding a convex obstacle.

show that the desired vehicle heading rate does not exceed the theoretical bound.

While the analysis is concerned with avoidance of a circular obstacle, implementation of the algorithm does not require knowledge the obstacle shape. In addition to the obstacle velocity, only the tangents from the vehicle to the obstacle are required. Hence, the algorithm can be used on obstacles of any shape, including concave shapes. Additional testing and analysis will, however, be required to investigate the behavior of the algorithm in such cases. As an example of such a case, a simulation of a successful avoidance maneuver around a concave obstacle has been presented.

This paper has analyzed a single obstacle scenario. In the presence of multiple obstacles, the algorithm will treat obstacles close to each other as one and move towards the outermost tangent. However, a thorough analysis of the behavior of the algorithm in a multi-obstacle scenario is beyond the scope of this paper and is left for future work. Similarly, the system behavior when the vehicle has more complex dynamics, like a vehicle with underactuated dynamics, is the topic of future research.

REFERENCES

[1] T. Statheros, G. Howells, and K. M. Maier, "Autonomous Ship Collision Avoidance Navigation Concepts, Technologies and Techniques," *Journal of Navigation*, vol. 61, no. 01, pp. 129–142, 2008.

[2] M. Hoy, A. S. Matveev, and A. V. Savkin, "Algorithms for collision-free navigation of mobile robots in complex cluttered environments: a survey," *Robotica*, vol. 33, no. 03, pp. 463–497, 2014.

[3] L. Lapierre, R. Zapata, and P. Lepinay, "Combined path-following and obstacle avoidance control of a wheeled robot," *The International Journal of Robotics Research*, vol. 26, no. 4, pp. 361–375, 2007.

[4] J. Canny and J. Reif, "New lower bound techniques for robot motion planning problems," in *Proc. 28th Annual Symposium on Foundations of Computer Science*, (Los Angeles, CA, USA), pp. 49–60, 1987.

[5] Y. Kim, D.-W. Gu, and I. Postlethwaite, "Real-time path planning with limited information for autonomous unmanned air vehicles," *Automatica*, vol. 44, no. 3, pp. 696–712, 2008.

[6] O. Khatib, "Real-time obstacle avoidance for manipulators and mobile robots," *The International Journal of Robotics Research*, vol. 5, no. 1, pp. 90–98, 1986.

[7] Y. Koren and J. Borenstein, "Potential field methods and their inherent limitations for mobile robot navigation," in *Proc. IEEE International Conference on Robotics and Automation (ICRA)*, (Sacramento, CA, USA), pp. 1398–1404, 1991.

[8] J. Borenstein and Y. Koren, "The vector field histogram–Fast obstacle avoidance for mobile robots," *IEEE Transactions on Robotics and Automation*, vol. 7, no. 3, pp. 278–288, 1991.

[9] D. Panagou, "Motion planning and collision avoidance using navigation vector fields," in *Proc. IEEE International Conference on Robotics & Automation (ICRA)*, (Hong Kong, China), pp. 2513–2518, 2014.

[10] D. Fox, W. Burgard, and S. Thrun, "The dynamic window approach to collision avoidance," *IEEE Robotics and Automation Magazine*, vol. 4, no. 1, pp. 23–33, 1997.

[11] B. O. H. Eriksen, M. Breivik, K. Y. Pettersen, and M. S. Wiig, "A modified dynamic window algorithm for horizontal collision avoidance for AUVs," in *Proc. 2016 IEEE Conference on Control Applications (CCA)*, (Buenos Aires, Brazil), pp. 499–506, 2016.

[12] P. Fiorini and Z. Shiller, "Motion planning in dynamic environments using velocity obstacles," *The International Journal of Robotics Research*, vol. 17, no. 7, pp. 760–772, 1998.

[13] A. Chakravarthy and D. Ghose, "Obstacle avoidance in a dynamic environment: A collision cone approach," *IEEE Transactions on Systems, Man, and Cybernetics Part A:Systems and Humans.*, vol. 28, no. 5, pp. 562–574, 1998.

[14] D. Wilkie, J. Van Den Berg, and D. Manocha, "Generalized velocity obstacles," in *Proc. IEEE/RSJ International Conference on Intelligent Robots and Systems,*, (St. Louis, MA, USA), pp. 5573–5578, 2009.

[15] J. van den Berg, J. Snape, S. J. Guy, and D. Manocha, "Reciprocal collision avoidance with acceleration-velocity obstacles," in *Proc. IEEE International Conference on Robotics and Automation (ICRA 2011)*, (Shanghai, China), pp. 3475–3482, 2011.

[16] E. J. Rodriguez-Seda, C. Tang, M. W. Spong, and D. M. Stipanovi, "Trajectory tracking with collision avoidance for nonholonomic vehicles with acceleration constraints and limited sensing," *The International Journal of Robotics Research*, vol. 33, pp. 1569–1592, Aug. 2014.

[17] A. S. Matveev, C. Wang, and A. V. Savkin, "Real-time navigation of mobile robots in problems of border patrolling and avoiding collisions with moving and deforming obstacles," *Robotics and Autonomous Systems*, vol. 60, no. 6, pp. 769–788, 2012.

[18] A. V. Savkin and C. Wang, "Seeking a path through the crowd: Robot navigation in unknown dynamic environments with moving obstacles based on an integrated environment representation," *Robotics and Autonomous Systems*, vol. 62, no. 10, pp. 1568–1580, 2014.

[19] A. V. Savkin and C. Wang, "A simple biologically inspired algorithm for collision-free navigation of a unicycle-like robot in dynamic environments with moving obstacles," *Robotica*, vol. 31, no. 6, pp. 993–1001, 2013.

[20] L. Pallottino, V. G. Scordio, E. Frazzoli, A. Bicchi, and E. Frazzoli, "Decentralized cooperative policy for conflict resolution in multi-vehicle systems," *IEEE Transactions on Robotics*, vol. 23, no. 6, pp. 1170–1183, 2007.

[21] E. J. Rodriguez-Seda, "Decentralized trajectory tracking with collision avoidance control for teams of unmanned vehicles with constant speed," in *Proc. American Control Conference*, (Portland, OR, USA), pp. 1216–1223, 2014.

[22] E. Lalish, K. A. Morgansen, and T. Tsukamaki, "Decentralized reactive collision avoidance for multiple unicycle-type vehicles," in *Proc. American Control Conference*, (Seattle, WA, USA), pp. 5055–5061, 2008.

[23] M. Breivik and T. I. Fossen, "Guidance laws for planar motion control," in *Proc. IEEE Conference on Decision and Control*, (Cancun, Mexico), pp. 570–577, 2008.